Ab initio electronic absorption spectra of *para*-nitroaniline in different solvents: intramolecular charge transfer effects

Matheus Máximo-Canadas[1], Itamar Borges Jr[1*]

[1]*Departamento de Química, Instituto Militar de Engenharia (IME), Praça General Tibúrcio, 80, Rio de Janeiro, RJ 22290-270, Brazil*

[*] Correspondence to: Itamar Borges Jr (E-mail: itamar@ime.eb.br)

ABSTRACT

Intramolecular charge transfer (ICT) effects of *para*–nitroaniline (*p*NA) in eight solvents (cyclohexane, toluene, acetic acid, dichloroethane, acetone, acetonitrile, dimethylsulfoxide, and water) of different polarities are investigated extensively. The second-order algebraic diagrammatic construction, ADC(2), *ab initio* wave function is employed with an implicit solvation method. We found that the pyramidal dihedral angle of the amine group depends on the solvent, decreasing with increased polarity. The first absorption band involves HOMO→LUMO $\pi\rightarrow\pi^*$ transitions with charge transfer from the amine and the benzene ring to the nitro group. ICT effects increase by 10% upon solvation in water compared to the gas phase. A second band of *p*NA is characterized for the first time. The brightest state of both bands depends on the polarity of the solvent. The second band is primarily a local excitation (LE) on the nitro group, including some CT from the amine group to the benzene ring that decreases with the solvent polarity. The LE character on the nitro group of the second band increases by 36% from the gas phase to water. A -0.32 eV redshift in the first band of cyclohexane increases to -0.84 eV in water, in agreement with experiment. The second band is redshifted by -0.21 eV for cyclohexane and -0.36 eV for water. An exponential correlation between the polarity and spectral properties is found, which saturates for solvents of intermediate polarities.

KEYWORDS

para–Nitroaniline, Intramolecular charge transfer (ICT), Electronic absorption spectra, Solvent effects, Second-order algebraic diagrammatic construction ADC(2)

1 INTRODUCTION

Push-pull molecules are organic systems bearing electron donor (D) and acceptor (A) groups, usually separated by a π-conjugated bridge in a D-π-A arrangement.[1] A push-pull configuration favors intramolecular charge transfer (ICT), which occurs when, upon excitation, electron density is redistributed in a molecule with an electron transfer from an electron-rich donor region to an electron-poor acceptor region taking place.[2] Besides the intrinsic scientific interest of ICT phenomena in different areas of chemistry, physics, biology, medicine, and engineering,[3–13] ICT has several applications, especially in organic electronics.[14–17]

The disubstituted benzene derivative *para–nitroaniline* (*p*NA) is a prototypical D-π-A push-pull molecule. It has an electron-donor amino group ($-NH_2$) and an electron-withdrawing nitro group ($-NO_2$) separated by a phenyl ring as a π-conjugated bridge (Scheme 1). Because of its relatively simple structure, it has been used to investigate different phenomena, including solvatochromism[18–22] and optical properties.[23–27] Although *p*NA is extensively studied, recent investigations of these properties highlight its continuing relevance.[28–32] Additionally, since *p*NA is a non-biodegradable pollutant,[33] highly toxic, mutagenic, and carcinogenic,[34,35] theoretical investigations of this molecule are particularly valuable.

Since most chemical reactions and spectroscopic measurements of molecules occur in a solvent, it is especially relevant to investigate these phenomena in this environment. In particular, the position, intensity, and shape of absorption and emission bands are influenced by the polarity of the solvent.[36] Concerning *p*NA, its solvent effects have been investigated theoretically, but not as comprehensively focusing in ICT phenomena as in the present work.[21,37–40] Frutos-Puerto employed sequential Quantum Mechanics/Molecular Mechanics (QM/MM) to investigate the origin of the nonlinear solvatochromic shift of *p*NA in solvents, i.e., the nonlinear dependence of the absorption energy on the composition of the cyclohexane and triethylamine (TEA) mixture.[21] They attributed this behavior to hydrogen bonds formed between *p*NA and TEA even at low TEA concentrations. Cardenuto also employed QM/MM to examine the electronic absorption spectrum of *p*NA in supercritical water.[38] Eriksen emphasized the inaccuracy of using Time-Dependent Density Functional Theory (TDDFT) with the CAM-B3LYP

exchange-correlation functional coupled to the polarizable embedding (PE) scheme to reproduce the measured solvatochromic shift in *p*NA in water and highlighted discrepancies in describing charge transfer effects of excited states employing TDDFT.[39] Sok employed molecular dynamics simulations of *p*NA with 150 water molecules and found that the primary contribution to the redshift in the spectrum are due to Coulombic interactions between *p*NA and water, combined with solute relaxation.[40] The contributions from solvent-induced shifts reflect the increased zwitterionic character of *p*NA upon solvation. Cabral et al. performed Born-Oppenheimer molecular dynamics of *p*NA in water, investigating the connection between dynamic changes in the molecular structure and the electronic features of charge transfer (CT) states of *p*NA in water.[37] The study examined the role of hydrogen bonds and electrostatic interactions in the spectral redshift.

Most of those works focused on a restricted set of solvents, in most cases, water. Therefore, systematically investigating a wider range of different solvents and polarities will allow a more comprehensive understanding of ICT and solvatochromism effects in this prototypical system.

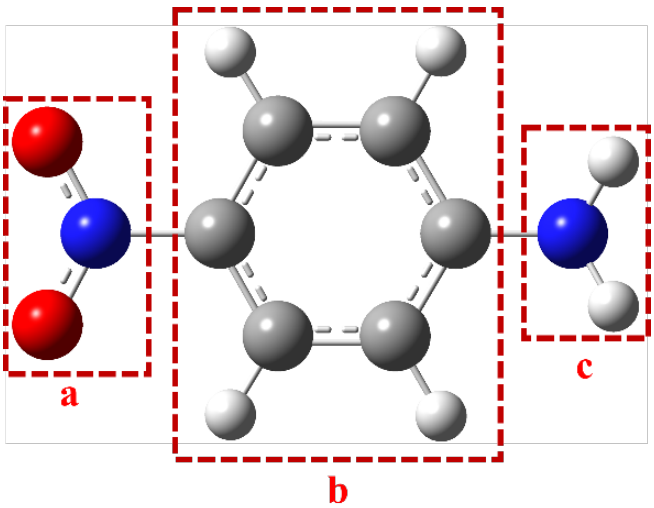

Scheme 1 The investigated system. The red dashed lines define the fragments, or regions, used for the charge transfer analysis described in the next section. Label “a” represents the nitro group, “b” the benzene ring, and “c” the amine group.

In this work, we employed the second-order algebraic diagrammatic construction (ADC(2)) *ab initio* wave function[41,42] to investigate comprehensively the absorption spectra and the intermolecular charge transfer (ICT) effects of the *p*NA molecule in eight solvents of varying polarities, namely, cyclohexane, toluene, acetic acid, dichloroethane, acetone, acetonitrile (CH_3CN), dimethylsulfoxide (DMSO), and water. Cyclohexane, toluene, and acetic acid are nonpolar solvents commonly used in organic chemistry for dissolving nonpolar compounds.[43] Dichloroethane and acetone have intermediate polarity. Acetonitrile, DMSO, and water are polar solvents.[44,45] Results will be compared with gas phase spectra.[32] The absorption spectra of *p*NA in cyclohexane, toluene, acetonitrile, DMSO, and water were measured before. Acetic acid, dichloroethane, and acetone were also studied because they are commonly used solvents and have intermediate polarities. A second absorption band, which was not measured or computed before, was found and comprehensively characterized.

2 METHODS

2.1 Computational Approach

The CAM-B3LYP exchange-correlation functional[46] and the def2-TZVPD Karlsruhe basis set[47,48] implemented in Gaussian 09[49] were used to optimize the singlet ground state (S_0) geometries of *p*NA for each solvent employing extremely tight optimization convergence criteria and no symmetry constraints. Minimum character and convergence to a planar structure (C_s point group) were confirmed by frequency calculations. The Conductor-like Polarizable Continuum Model, CPCM[50,51] in Gaussian 09, was employed to include solvent effects in the geometry optimization.

The investigated solvents are, in order of increasing polarity (relative permittivity or dielectric constant ε_r between parentheses): cyclohexane (2.017), toluene (2.374), acetic acid (6.2528) dichloroethane (10.125), acetone (20.493), acetonitrile (CH_3CN, 35.688), dimethylsulfoxide (DMSO, 46.826), and water (78.355).

We previously computed[32] ten gas-phase vertical singlet excited states of the *p*NA molecule using the resolution of identity (RI) algebraic diagrammatic construction method of the second-order, ADC(2),[41,42] an *ab initio* wave function, with the def2-

TZVPD basis set. For these calculations, the Turbomole v 6.6 program was employed.[52,53] The vertical excitations, including the solvent effects of this work were computed employing the Conductor-like Screening Model (COSMO) continuum model[54] with the state-specific approach[55] using the converged CAM-B3LYP solvated geometries. The vertical calculations employing the COSMO solvent model were performed also with Turbomole v6.6.

The ADC(2) *ab initio* wave function is known for accurately describing excited states,[56–59] including charge transfer[7,60–65] and solvent effects.[65–68] Unlike TDDFT, ADC(2) avoids the arbitrariness of the choice of exchange-correlation functionals and the inherent limitations in describing charge transfer effects.[8,61] Previous studies have demonstrated that ADC(2), combined with the modeling of solvation effects using COSMO, provides a well-balanced description of both locally excited (LE) and charge transfer (CT) states.[65] In this work, spectra were convoluted with Gaussian curves using a line width of 0.5 eV. The highest intensity of the absorption band in each case was normalized to 1.0.

2.2 Charge transfer analysis

The charge transfer (CT) in the excited states was characterized by a transition density matrix analysis and Natural Transition Orbitals (NTOs).[69] This analysis employed the TheoDORE package.[70,71] The NTOs are valuable constructs for elucidating molecular electronic transitions. When more than a pair of NTOs significantly contribute to a transition, a transition amplitude (λ) is calculated to indicate the magnitude of a specific NTO pair contribution to the overall electronic transition. This λ, in turn, quantifies the weight of a particular pair of NTOs in describing the redistribution of electron density after the transition. Only a few NTOs usually have appreciable amplitudes, which concisely represent the excitation process.[70] Consequently, NTOs eliminate the ambiguity associated with a specific choice of molecular orbitals,[72] thus allowing an accurate interpretation of the nature of electronic excitations.

For a molecule with two or more distinct regions or fragments, such as A and B, the representation of the transition matrix elements for a transition from the ground state to the nth excited state (denoted as D_{rs}^{0n}) can be expressed using a basis set of localized

orbitals according to Equation (1). The $\hat{\varepsilon}_{rs}$ is the excitation operator involving the r and s orbitals,

$$D_{rs}^{0n} = \langle 0|\hat{\varepsilon}_{rs}|n\rangle \quad (1)$$

The charge-transfer number (Ω_{AB}^{n}) for the excitation is defined by summing up the contributions from the regions A and B of the system, as indicated in Equation (2) below. The S matrix is the orbital overlap, and the summations are performed over the basis functions associated with atoms μ and ν:

$$\Omega_{AB}^{n} = \frac{1}{2}\sum_{\mu\in A}\sum_{\nu\in B}\left[(D^{0n}S)_{\mu\nu}(SD^{0n})_{\mu\nu} + D_{\mu\nu}^{0n}(SD^{0n}S)_{\mu\nu}\right] \quad (2)$$

When $A \neq B$, Ω_{AB}^{n} represents the weight of charge transfer (CT) from region A to B. In contrast, when $A = B$, Ω_{AA}^{n} is the weight of locally excited (LE) transitions on A. The overall charge transfer number $q(CT)$ for a system with multiple fragments or regions is defined by summing over the off-diagonal elements according to Equation (3) below. The Ω^{n} term is the normalization factor corresponding to the total sum of charge transfer numbers for all A and B pairs. The CT descriptor reflects the cumulative weight of configurations where the initial and final orbitals are located on distinct fragments,

$$q(CT) = \frac{1}{\Omega^{n}}\sum_{A}\sum_{B\neq A}\Omega_{AB}^{n} \quad (3)$$

When $q(CT) = 1$, the state has complete charge separation, while $q(CT) = 0$ describes a locally excited or Frenkel excitonic state.[73] The CT analysis employed the three molecular regions defined in Scheme 1. The CT for each transition was decomposed and named according to the following labels: CT from the nitro and the ring to the amine group (*ACT*); CT from the amine and the ring to the nitro group (*NCT*); and CT from the side groups nitro and amine to the benzene ring (*RCT*). It was found a local excitation character in the three molecular regions, named the amine group (*ALE*), nitro group (*NLE*), and the benzene ring (*RLE*) charge transfer.

3 RESULTS AND DISCUSSION

3.1 Geometries

The coordinates of the optimized geometries of *p*NA ground state in each solvent are collected in Table S18 of the Supplementary Material (SM). The main difference between the experimental crystal data of *p*NA[74–76] and the converged gas phase geometry is that, for CAM-B3LYP//def2-TZVPD, the amino (NH_2) group is slightly pyramidal (16.9°). In contrast, in the crystal this group is coplanar with the rest of the molecule due to the intermolecular interactions, as found before.[21]

The optimized ground state geometry in different solvents have an interesting trend. In more apolar solvents, the geometry closely resembles the crystal structure,[74–76] while in more polar solvents, there is an increase in the pyramidal dihedral angle of the amine group. This finding can be rationalized by examining two molecular resonance structures, the neutral *p*NA structure and the zwitterionic structure[77] indicated in Scheme 2. In more polar solvents, the zwitterionic structure becomes more pronounced, thus modifying the molecular geometry because the positive charge on the nitrogen's amine interacts more strongly with the negative partial charges of the polar solvent molecules, favoring the zwitterionic form, hence a smaller angle. Therefore, by increasing the polarity of the solvent, we obtain the decreasing dihedral angles (between parentheses): cyclohexane (15.3°), toluene (15.0°), acetic acid (12.6°), dichloroethane (11.7°), acetone (10.7°), acetonitrile (10.2°), dimethylsulfoxide (10.1°), and water (9.8°).

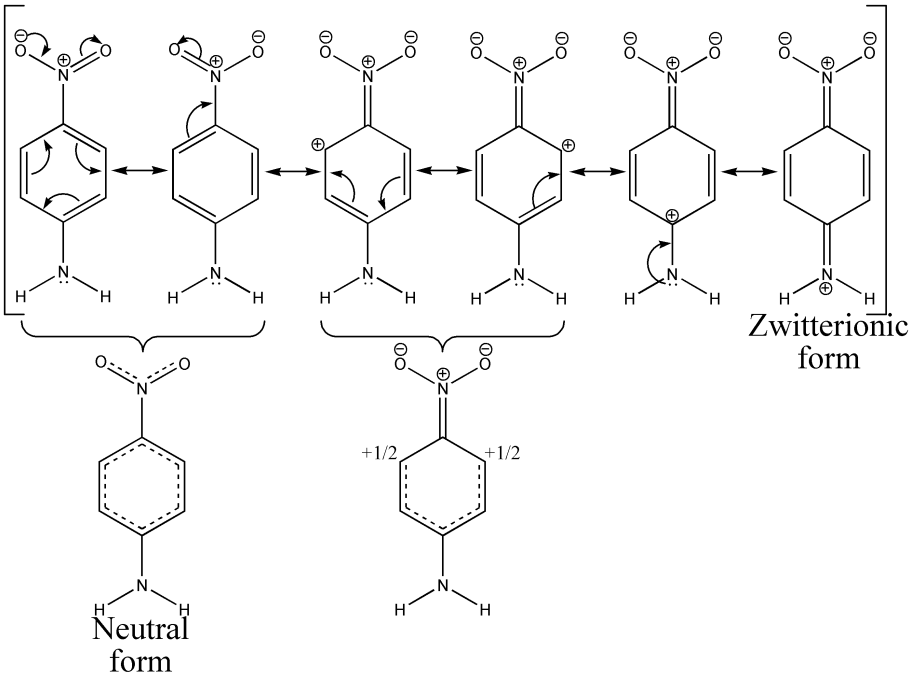

Scheme 2 The *p*NA resonance structures with their hybrids: neutral form and zwitterionic form. (Adapted from Ref. [77].)

3.2 The solvent effect in the absorption spectra

Characterizing charge transfer effects in solvent excited states is crucial for rationalizing the electronic and molecular processes occurring during these transitions and the impact of the environment. Figure 1 presents the different contributions from charge transfer (CT) and localized excitations (LE) found in the first ten electronic transitions in gas phase found before.[32] The brightest states of each band in the gas phase, oscillator strengths, and the NTOs for the transitions are also shown. Figures S2 to S9 of the SM show similar representations for each solvent. The explicit values of these decompositions in gas and solvent phase are presented in Tables S9 to Table S17 of the SM.

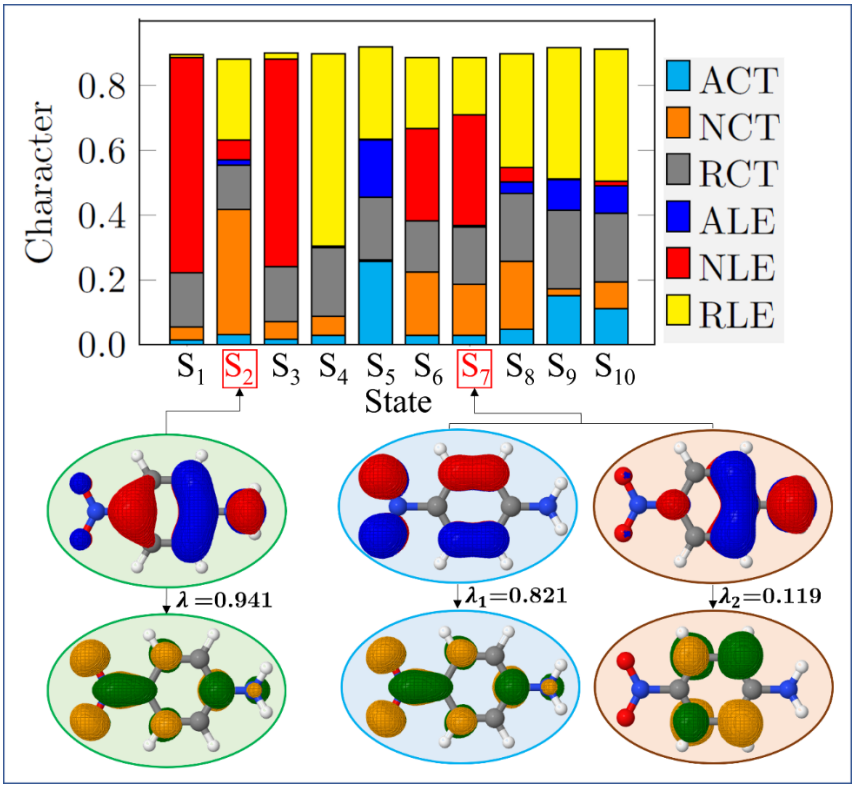

Figure 1. ADC(2)//def2-TZVPD charge transfer (CT) analysis of the first ten transitions of *p*NA gas phase. Gas phase data from Ref.[32] The following notation was defined for describing each contribution: *ACT* – CT from the nitro and the ring to the amine group; *NCT* – CT from the amine and the ring to the nitro group; and *RCT* – CT from the side groups nitro and amine to the benzene ring. Also, we define the local excitations (LE) *ALE* – LE on the amino group, *NLE* – LE on the nitro group, and *RLE* – LE on the benzene ring. The transition S_2 and S_7 are the brightest states of the first and second bands, respectively. The corresponding natural transition orbitals and transition weight (λ) are shown.

The bright state of the first band is the S_2 transition in both gas and low (cyclohexane and toluene) and intermediate polarity solvents (acetic acid and dichloroethane, but not acetone). For acetone and more polar solvents (acetonitrile, DMSO, and water), the bright state of the first band is the S_1. The acetone's polarity (ε_r = 20.493), although lower than the more polar solvents (e.g., acetonitrile with ε_r = 35.688), is already considered polar.

The brightest state of the first band in gas or any solvent is a HOMO→LUMO $\pi\rightarrow\pi^*$ transition, which preserves the gas phase CT character from the amine and the ring

to the nitro group. The charge transfer number $q(NCT)$ equals $0.388e$ in the gas phase, but increases with the polarity of the solvent as expected from chemical intuition: cyclohexane ($0.404e$), toluene ($0.407e$), acetic acid ($0.423e$), dichloroethane ($0.426e$), acetone ($0.429e$), acetonitrile ($0.431e$), dimethylsulfoxide ($0.431e$), and water ($0.432e$) – see the $q(NCT)$ values for each solvent in Tables S9 to S17. Therefore, a higher polarity of the solvent enhances charge transfer to the strongly accepting nitro group. In nonpolar solvents, such as cyclohexane and toluene, electrostatic interactions of the solvent with the nitro group are far less critical, resulting in slightly smaller $q(NCT)$ values. For these bright states, the LE character on the benzene ring decreases with solvent polarity, from gas phase ($q(RLE) = 0.250e$) to water ($0.202e$), because more polar solvents have more ICT. In water, for instance, the increase of the $q(NCT)$ and decrease of the $q(RLE)$ values increase the total $q(CT)$ value from $0.631e$ in gas phase to $0.659e$ in water.

The brightest state of the second band in the gas phase is the S_7.[32] For low polarity solvents (cyclohexane and toluene) and intermediary ones (acetic acid, dichloroethane, and acetone), the brightest state of the second band is also S_7. For more polar solvents (acetonitrile, DMSO, and water), the brightest of the second band is the S_6 transition instead. HOMO-2-LUMO transitions dominate all these excitations – see Tables S1 to Table S8. They involve two NTOs, the dominant one (higher λ) governed by a LE on the nitro group and the second contribution (lower λ) by a CT from the amine group to the benzene ring. The weight of the second NTOs pair decreases with the polarity of the solvent, ranging from 11.9% in the gas phase to 5.0% in acetonitrile (CH_3CN), becoming negligible for DMSO and water. Accordingly, $q(ACT)$ decreases and $q(NLE)$ increases from gas phase ($0.029e$ and $0.344e$, respectively) to water ($0.023e$ and $0.534e$, respectively). Consequently, the total $q(CT)$ values follow this trend, decreasing from $0.414e$ in the gas phase to $0.324e$ in the water, which indicates a more localized excitation. Figure 2 depicts this behavior, highlighting the brightest state in the first and second absorption bands for each solvent. The corresponding transition energies are also presented in the upper panel. A higher solvent polarity decreases the transition energy, a patent solvatochromism effect because polar solvents stabilize the excited state through favorable interactions with the nitro group.

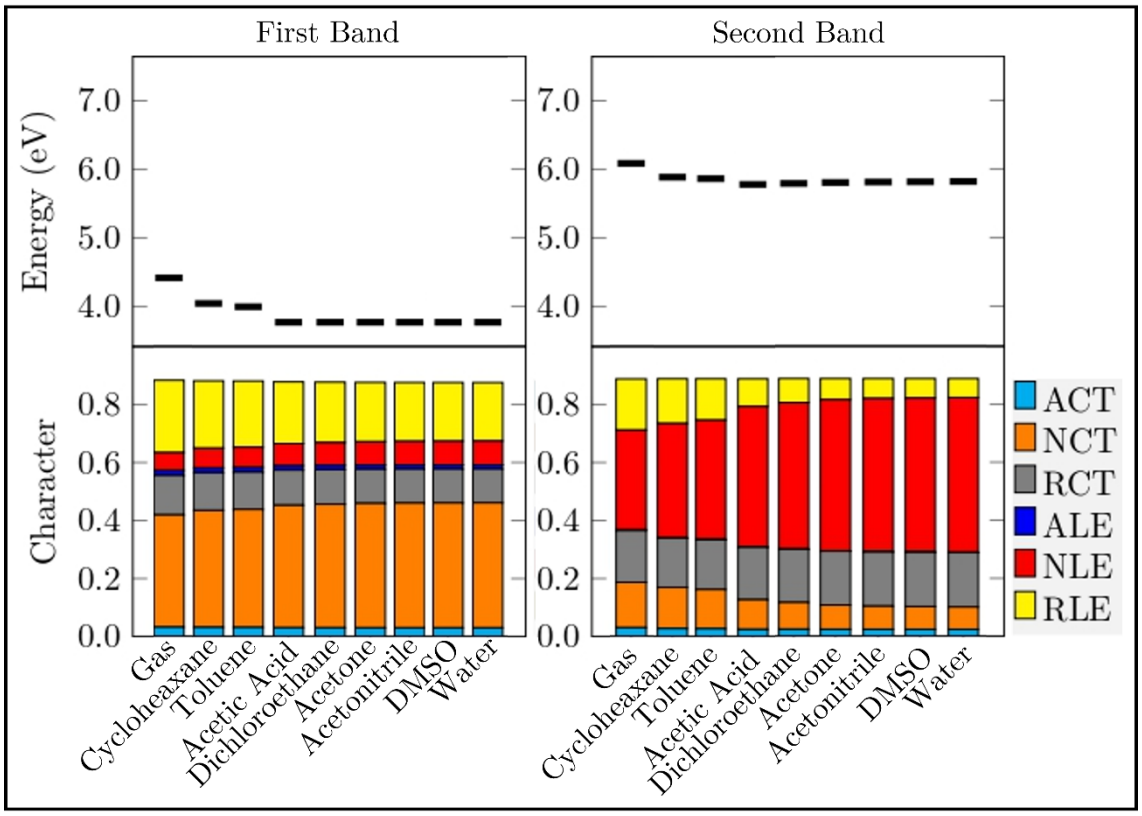

Figure 2. ADC(2) transition energies (upper panel) and the decomposition character (lower panel) of the brightest state of the first (left) and second (right) band of the absorption spectra for each solvent: cyclohexane (S_2 and S_7), toluene (S_2 and S_7), acetic acid (S_2 and S_7) dichloroethane (S_2 and S_7), acetone (S_1 and S_7), acetonitrile (CH_3CN, S_1 and S_6), dimethylsulfoxide (DMSO, S_1 and S_6), and water (S_1 and S_6). The following notation was used: *ACT* – CT from the nitro and the ring to the amine group; *NCT* – CT from the amine and the ring to the nitro group; *RCT* – CT from the side groups nitro and amine to the benzene ring; *ALE* – LE on the amino group; *NLE* – LE on the nitro group; and *RLE* – LE on the benzene ring. Gas phase theoretical results data from Ref.[32]

Table 1 presents the transition energies (ΔE), optical oscillator strengths (f), and the dominant contribution to the character of all the singlet states. The corresponding $q(CT)$ values for all solvents are presented in Table S1 to Table S8 of the SM.

Table 1. Computed properties of *p*NA for each solvent. Optimized CAM-B3LYP//def2-TZVPD geometries for each solvent using the CPCM solvation method.

Solvent[a]	E_{gap} [b]	E_{B1} [c]	E_{B2} [c]
Gas Phase[32]	10.416	4.415 (S_2)	6.086 (S_7)
Cyclohexane	10.219	4.017 (S_2)	5.886 (S_7)
Toluene	10.173	3.967 (S_2)	5.870 (S_7)
Acetic Acid	9.949	3.730 (S_2)	5.797 (S_7)
Dichloroethane	9.875	3.652 (S_2)	5.775 (S_7)
Acetone	9.804	3.579 (S_1)	5.757 (S_7)
Acetonitrile	9.772	3.546 (S_1)	5.748 (S_6)
DMSO	9.761	3.535 (S_1)	5.746 (S_6)
Water	9.747	3.520 (S_1)	5.742 (S_6)

[a] The investigated solvents, from top to bottom, in decreasing order of polarity.

[b] HOMO-LUMO gap energies in eV.

[c] ADC(2) transition energies *p*NA (in eV) of the brightest state (between parentheses) of the first and second bands represented by E_{B1} and E_{B2}, respectively.

The polarity of the solvent also influences the HOMO-LUMO gap, which decreases with increasing polarity (Table 1). The HOMO→LUMO transition, the brightest state of the first band, is a CT from the amine and the ring to the nitro group, as discussed earlier. Polar solvents have permanent dipoles, which interact electrostatically with the polarizable electron density of the CT state. This stabilizing interaction between the solvent and the CT state reduces the energy required for the HOMO–LUMO transition, thus favoring energetically the transition. The same occurs with the ADC(2) transition energies – see Table 1. Furthermore, as shown in Tables S1 to S8, we found that, upon solvation, specific gas phase *p*NA states become so stabilized that they significantly decrease their transition energies. For instance, in cyclohexane, the S_{10} state (6.421eV) has lower energy than S_9 (6.423eV), and in S_{13} (6.894eV) is less than S_{12} (6.935eV). For toluene, S_{13} has lower energy than S_{12}. This trend occurs in all solvents except acetone and acetonitrile.

When the solvent polarity increases, there is a slight increase in the optical oscillator strength f of the brightest state in the first band. The oscillator strength

increases from 0.491 in cyclohexane to 0.497 in water. In contrast, the optical oscillator strength of the brightest state in the second band decreases as the solvent polarity increases from 0.348 in cyclohexane to 0.282 in water, indicating that polar solvents decrease appreciably the transition probability of this band. Therefore, the solvent polarity enhances the intensity of CT transitions in the first band while reducing the intensity of transitions in the second.

The computed gas phase[32] and solvated ADC(2)//def2-TZVPD vertical spectra are depicted in Figure 3. The available experimental spectra in cyclohexane, toluene, acetonitrile, DMSO, and water are also shown, as all the solvents together in Figure 3(F). The solvated *p*NA spectra in acetic acid, dichloroethane, and acetone, which do not have available experimental data, are presented in Figure S1 of the SM.

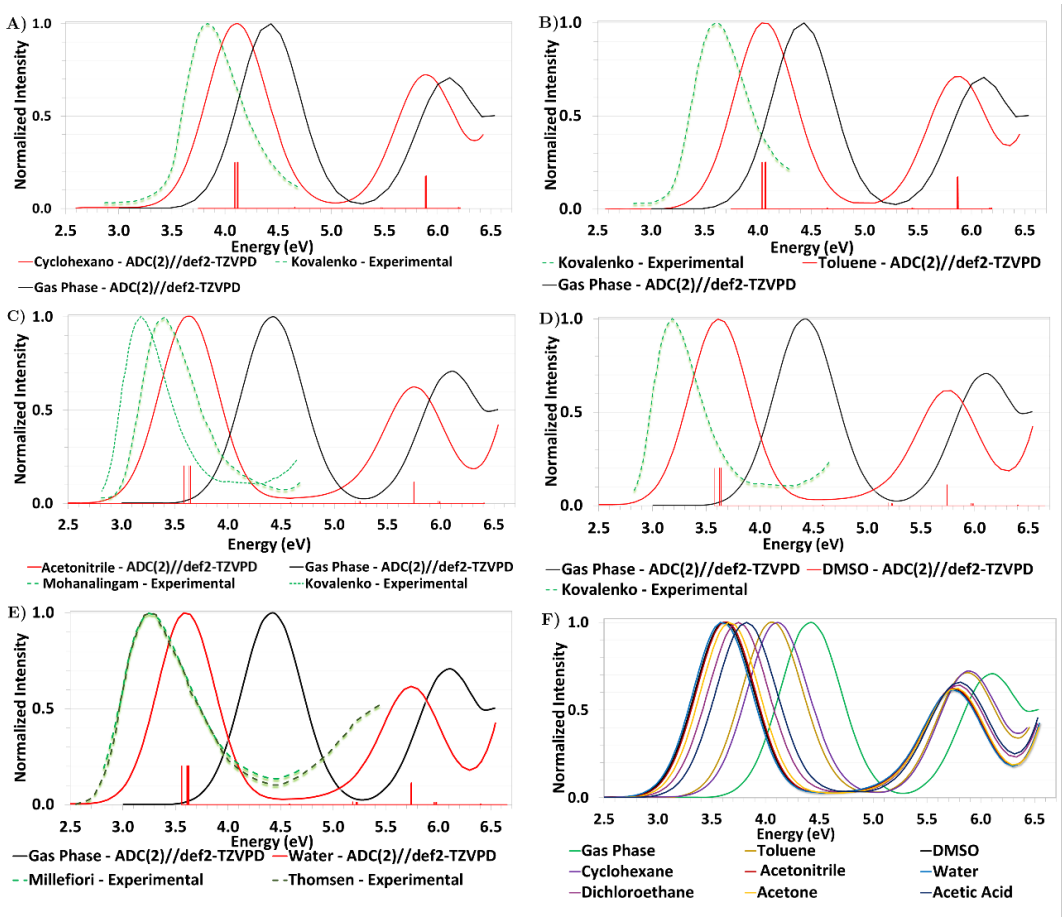

Figure 3. *p*NA absorption spectra in solvent and gas phase. From A) to E), the red lines are the computed ADC(2)//def2-TZVPD solvated spectra. Black lines represent the gas phase spectrum,[31] whereas the dashed green curves are the experimental data.[22,78–80] ADC(2) results for A) cyclohexane and experiment,[78] B) toluene and experiment,[78] C)

acetonitrile (CH_3CN) and experiment,[79] D) DMSO and experiment,[78] and E) water and experiment.[22,80] The F) panel presents the computed ADC(2) gas phase and solvated spectra. The spectra were convoluted with Gaussian curves with a line width of 0.5 eV. The *y*-axis was normalized to 1.0 at the energy of the brightest absorption peak.

The brightest state within each band is not the only one having appreciable oscillator strength – see Table S1 to Table S8 of the SM. Consequently, when convolving these excited states with Gaussian curves using a linewidth of 0.5 eV for producing the spectra in Figure 3, the bands appear with a maximum energy that differs from the energy of the brightest state.

We found an expected dependence of the *p*NA electronic absorption spectra on the polarity of the solvent. The first band absorption maximum energy has a redshift with magnitude increasing with the polarity of the solvent – the redshift varies from 0.32 eV in low polar cyclohexane to 0.84 eV for the high polar water. These findings are in good agreement with the experiment regarding the first band, which found 0.42 eV (cyclohexane) and 0.99 eV (water). There is also a redshift in the second band (not measured or computed before), with the magnitude also increasing with the polarity of the solvent. However, this shift has a smaller magnitude than for the first band: 0.21 eV for cyclohexane and 0.36 eV for water. The redshifts of both bands for the solvents of intermediate polarities have values between the redshifts of cyclohexane and water.

The electron density on the nitro group associated with the CT (first band) and LE (second band) transitions is affected by the polarity of the solvent. In polar solvents, dipole interactions can stabilize these densities on a nitro group, leading to lower transition energies resulting in a redshift of the absorption bands. As discussed previously, the second band's relative intensity slightly decreases with polarity (about 14% from cyclohexane to water).

The comparison of the experimental spectra and the ADC(2) ones reveals an overestimation of the ADC(2)//def2-TZVPD maximum energy of the first band – see Table 1. For *p*NA in cyclohexane, Kovalenko obtained a maximum energy of 3.835 eV,[78] whereas our findings indicate a slightly higher value of 4.017eV (0.182 eV difference). Similarly, toluene has a 0.352 eV difference between Kovalenko (3.615 eV) and our value

(3.967 eV). Acetonitrile differs (0.134 eV) from Kovalenko[78] and Mohanalingam,[79] who reported 3.412 eV, while our analysis yields a slightly higher value of 3.546 eV. DMSO showcases the most significant discrepancy of all solvents computed by other authors (0.351 eV), with Kovalenko[78] reporting 3.184 eV compared with our value of 3.535 eV. Millefiori [22] and Thomsen[80] reported 3.246 eV and 3.263 eV for water, respectively, while our investigation found 3.520 eV (0.257 eV higher than Thomsen's).

As discussed in the Introduction, the first electronic band of the *p*NA has been extensively theoretically investigated. The previous studies[21,38,39] also found that the brightest transition is the S_2, a $\pi \rightarrow \pi^*$ excitation dominated by a CT from the amino to the nitro group. This charge transfer nature means that the properties of the transition are affected by the solvent polarity, thus producing a solvatochromic shift, as we have just presented and was found before.[21]

It has been found that explicit models incorporating hydrogen bonds in most cases improve the theoretical prediction of the absorption band redshift of *p*NA in a solvent.[21,37,38,81] In water, Cabral et al. obtained an energy of 3.5 eV for the first band,[37] consistent with our findings. For cyclohexane, Frutos-Puerto obtained an energy of 4.32 eV,[21] whereas our result was 4.017 eV, in better agreement with experiment (3.835 eV[78]). Therefore, despite the lack of explicit hydrogen bonds in our implicit solvent model, our results have a good accuracy, showing better agreement with experiment than some explicit solvent studies.

To examine an eventual correlation between polarity and spectral properties, we plotted in Figure 4 ADC(2)//def2-TZVPD the dielectric constants of the solvents and properties showed in Table 1. An exponential fit of the data was used. The HOMO–LUMO gap (E_{gap}) energy exhibited a good fitting. The R^2_{adj} of 0.99989 suggests alignment between predicted and observed values. The small value of χ^2_{red} (6.559×10^{-5}) indicates that the function fits the data with a high accuracy. The RMSE is very small, 0.00256 eV. The energy of the brightest state in the first (E_{B1}) and second (E_{B2}) bands were also evaluated and yielded good results – see Figure 4.

The exponential fits display a saturation effect in all cases, with the property values becoming less sensitive to the polarity of the solvent until, for intermediate solvents, the property reaches a plateau. The investigated properties reach this saturation for dielectric constants of 20 and 30, corresponding to solvents of medium polarity.

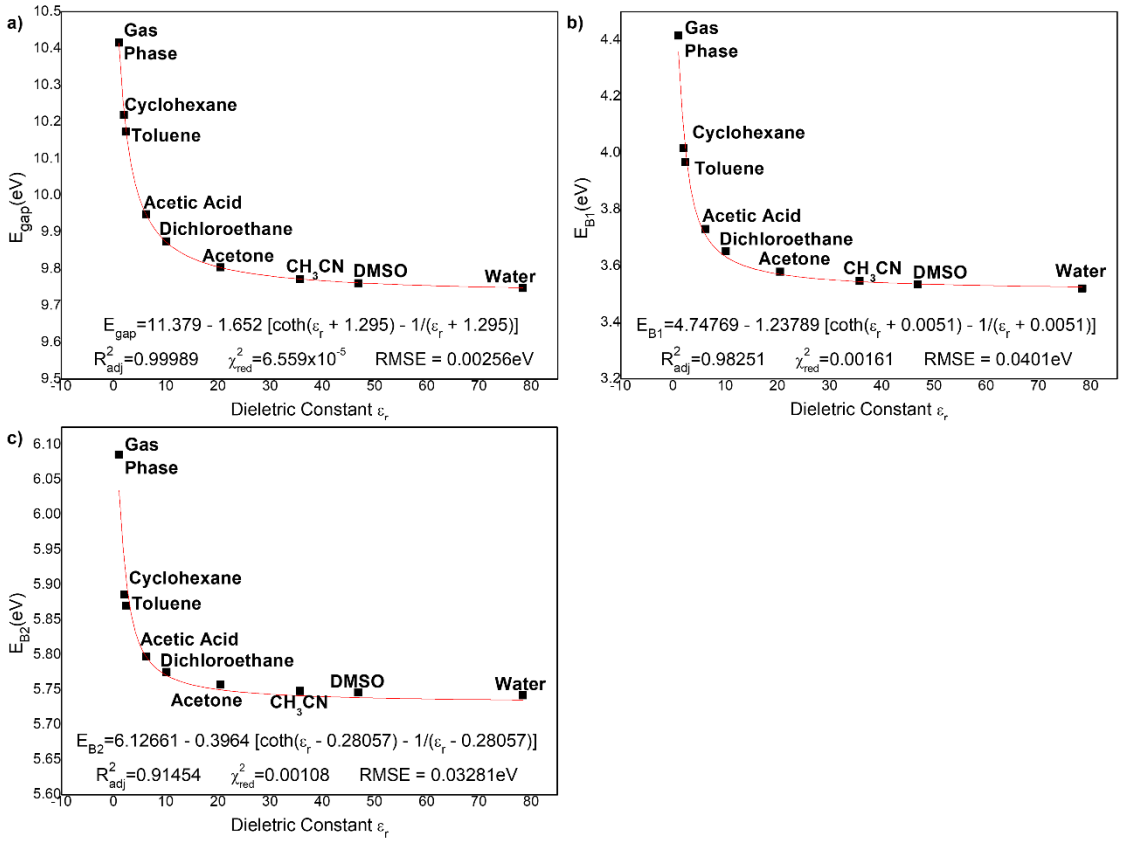

Figure 4. Relation between dielectric constant (ε_r) and the molecular properties a) HOMO-LUMO gap energy (E_{gap}), b) first band maximum energy (E_{B1}), and g) second band maximum energy (E_{B2}). Evaluation metrics for each model: Adjusted coefficient of determination (R^2_{adj}), Reduced chi-squared (χ^2_{red}), and Root-mean-square error (RMSE).

4 CONCLUSIONS

We investigated the solvent effect on the electronic properties of *p*NA employing eight solvents with different polarities. The solvents in order of increasing polarity were cyclohexane, toluene, acetic acid, dichloroethane, acetone, acetonitrile (CH_3CN), dimethylsulfoxide (DMSO), and water. Using the CPCM continuum solvation model, the pyramidal dihedral angles of the amine group in the optimized ground geometries of the *p*NA in different solvents reveal a correlation with solvent polarity. For the more polar

solvents, the dihedral angle increases due to the prominence of the zwitterionic structure in polar solvents.

The ADC(2)//def2-TZVPD method was used to compute the electronic vertical transitions using the solvated geometries, and the solvent effect in the transitions was modeled using the COSMO-RS continuum model. The solvated electronic transitions were characterized and quantified concerning charge transfer (CT) and locally excited (LE) properties. The brightest state of the first band is a HOMO→LUMO $\pi\rightarrow\pi^*$ transition characterized by CT from the amine and benzene ring to the highly electron-withdrawal nitro group. This CT effect is enhanced in more polar solvents, while nonpolar solvents resulting in a relatively unchanged CT compared with previous gas phase results. We also identified a second band in the absorption spectrum, not experimentally or theoretically characterized before. The dominant transition in the second band is a HOMO–2→LUMO transition with a larger solvent polarity increasing the locally excited (LE) character of the nitro group in the *p*NA molecule.

We found a redshift of the transition energies, with its magnitude increasing with the dielectric constant of the solvent. The ADC(2)//def2-TZVPD results slightly overestimated the maximum of the experimental band. The polarity of the medium also affects the HOMO-LUMO gap, which decreases with increasing polarity due to the more favorable electrostatic interactions between the more polar solvents and the polarizable electron density of the CT state.

We also investigated the correlation between the solvent polarity given by the dielectric constant (ε_r) and the molecular properties HOMO-LUMO gap energies and the ADC(2) transitions energies brightest states of the first and second bands. We found these properties exhibited a saturation effect, with properties becoming less sensitive for solvents of intermediate polarity, corresponding to dielectric constants in the range from 20 to 30.

In this work, we have made a comprehensive study of the solvent effects on the electronic transitions of the *p*NA molecule, focusing on charge transfer effects. Solvents with all polarity ranges have been investigated, and their impact on the transition

properties was rationalized. A second band, not previously computed or measured before, was found and characterized.

ACKNOWLEDGMENTS

I.B. thanks the Brazilian agencies Conselho Nacional de Desenvolvimento Científico e Tecnológico (CNPq) through research grants 304148/2018–0 and 409447/2018–8, and Fundação Carlos Chagas Filho de Amparo à Pesquisa do Estado do Rio de Janeiro (FAPERJ) through grant E-26/201.197/2021 for the support of this research. M.M-C. thanks Coordenação de Aperfeiçoamento de Pessoal de Nível Superior (Capes) for a Ph.D. scholarship. Support for this research from the National Institute of Science and Technology on Molecular Sciences (INCT-CiMol) grant CNPq 406804/2022-2, and Nano Network grant FAPERJ E-26/200.008/2020, is also greatly acknowledged. It is a great pleasure to dedicate this paper to the 80th anniversary of Hans Lischka. For almost 20 years, the second author (I. B.) has had the pleasure to collaborate with Hans, learn a great deal from him and share his friendship. Some results of this fruitful collaboration are cited in this paper. We are looking forward for the next years of collaboration!

CONFLICT OF INTEREST STATEMENT

The authors declare no conflicts of interests.

DATA AVAILABILITY STATEMENT

The data that support the findings of this study are available in the supplementary material of this article. Additional data are available in GitHub and Zenodo[82] and can be accessed via https://doi.org/10.5281/zenodo.10524944.

ORCID

Matheus Máximo-Canadas https://orcid.org/0009-0003-3029-1902

Itamar Borges Jr https://orcid.org/0000-0002-8492-1223

REFERENCES

1. F. Bureš, *RSC Adv*, **2014**, 4, 58826–58851.

2. R. Misra and S. P. Bhattacharyya, *Intramolecular Charge Transfer*, Wiley-VCH Verlag GmbH & Co. KGaA, Weinheim, **2018**.

3. M. Ipuy, C. Billon, G. Micouin, J. Samarut, C. Andraud and Y. Bretonnière, *Org Biomol Chem*, **2014**, 12, 3641–3648.

4. S. H. Gao, M. S. Xie, H. X. Wang, H. Y. Niu, G. R. Qu and H. M. Guo, *Tetrahedron*, **2014**, 70, 4929–4933.

5. R. M. Jones, L. Lu, R. Helgeson, T. S. Bergstedt, D. W. McBranch and D. G. Whitten, *Proc Natl Acad Sci U S A*, **2001**, 98, 14769–14772.

6. R. Ziessel, G. Ulrich, A. Harriman, M. A. H. Alamiry, B. Stewart and P. Retailleau, *Chemistry – A European Journal*, **2009**, 15, 1359–1369.

7. A. A. J. Aquino, I. Borges, R. Nieman, A. Köhn and H. Lischka, *Physical Chemistry Chemical Physics*, **2014**, 16, 20586–20597.

8. T. Stein, L. Kronik and R. Baer, *J Am Chem Soc*, **2009**, 131, 2818–2820.

9. S. Karak, F. Liu, T. P. Russell and V. V. Duzhko, *ACS Appl Mater Interfaces*, **2014**, 6, 20904–20912.

10. G. Turkoglu, M. E. Cinar and T. Ozturk, *Molecules 2017, Vol. 22, Page 1522*, **2017**, 22, 1522.

11. G. Archetti, A. Abbotto and R. Wortmann, *Chemistry – A European Journal*, **2006**, 12, 7151–7160.

12. S. jie Xu, Z. Zhou, W. Liu, Z. Zhang, F. Liu, H. Yan, X. Zhu, S. Xu, Z. Zhou, W. Liu, Z. Zhang, X. Zhu, F. Liu and H. Yan, *Advanced Materials*, **2017**, 29, 1704510.

13. S. Paek, J. K. Lee and J. Ko, *Solar Energy Materials and Solar Cells*, **2014**, 120, 209–217.

14. X. Liang and Q. Zhang, *Sci China Mater*, **2017**, 60, 1093–1101.

15. Y. Li, T. Liu, H. Liu, M.-Z. Tian and Y. Li, *Acc Chem Res*, **2014**, 47, 1186–1198.

16. C. Moon, K. Suzuki, K. Shizu, C. Adachi, H. Kaji and J. Kim, *Advanced Materials*, **2017**, 29.

17. I. Borges, R. M. P. O. Guimarães, G. Monteiro-de-Castro, N. M. P. Rosa, R. Nieman, H. Lischka and A. J. A. Aquino, *J Comput Chem*, **2023**, 44, 2424–2436.

18. O. S. Khalil, C. J. Seliskar and S. P. McGlynn, *J Chem Phys*, **2003**, 58, 1607.

19. T. P. Carsey, G. L. Findley and S. P. McGlynn, *J Am Chem Soc*, **1979**, 101, 4502–4510.

20. D. Kosenkov and L. V. Slipchenko, *Journal of Physical Chemistry A*, **2011**, 115, 392–401.

21. S. Frutos-Puerto, M. A. Aguilar and I. Fdez Galván, *Journal of Physical Chemistry B*, **2013**, 117, 2466–2474.

22. S. Millefiori, G. Favini, A. Millefiori and D. Grasso, *Spectrochim Acta A*, **1977**, 33, 21–27.

23. C. E. Agudelo-Morales, O. F. Silva, R. E. Galian and J. Pérez-Prieto, *ChemPhysChem*, **2012**, 13, 4195–4201.

24. R. Zaleśny, *Chem Phys Lett*, **2014**, 595–596, 109–112.

25. B. Champagne, *Chem Phys Lett*, **1996**, 261, 57–65.

26. A. Nayak, J. Park, K. De Mey, X. Hu, T. V. Duncan, D. N. Beratan, K. Clays and M. J. Therien, *ACS Cent Sci*, **2016**, 2, 954–966.

27. J. N. Woodford, M. A. Pauley and C. H. Wang, *Journal of Physical Chemistry A*, **1997**, 101, 1989–1992.

28. T. Siva, P. Thirumurugan, P. Jeyanthi and A. Ramadoss, *Results in Surfaces and Interfaces*, **2022**, 8, 100069.

29. M. Rashid and S. Sabir, *J Dispers Sci Technol*, **2009**, 30, 297–304.

30. A. A. I. Abed-Elmageed, M. S. Zoromba, R. Hassanien and A. F. Al-Hossainy, *Opt Mater (Amst)*, **2020**, 109, 110378.

31. Z. Mehrani, H. Ebrahimzadeh, A. R. Aliakbar and A. A. Asgharinezhad, *Microchimica Acta*, **2018**, 185, 1–9.

32. M. Máximo-Canadas and I. Borges, *SSRN*, **2023**.

33. Y. S. Zhao, C. Sun, J. Q. Sun and R. Zhou, *Sep Purif Technol*, **2015**, 142, 182–188.

34. R. Benigni and L. Passerini, *Mutation Research/Reviews in Mutation Research*, **2002**, 511, 191–206.

35. W. Xie, J. Zhang, Y. Zeng, H. Wang, Y. Yang, Y. Zhai, D. Miao and L. Li, *Anal Bioanal Chem*, **2020**, 412, 5653–5661.

36. et al. Mihaela HOMOCIANU, *Journal of Advanced Research in Physics*, **2017**, 2.

37. B. J. C. Cabral, K. Coutinho and S. Canuto, *Journal of Physical Chemistry A*, **2016**, 120, 3878–3887.

38. M. H. Cardenuto, K. Coutinho, B. J. C. Cabral and S. Canuto, *Advances in Quantum Chemistry*, **2015**, 71, 323–339.

39. J. J. Eriksen, S. P. A. Sauer, K. V. Mikkelsen, O. Christiansen, H. J. A. Jensen and J. Kongsted, *Molecular Physics* , **2013**, 111, 1235–1248.

40. S. Sok, S. Y. Willow, F. Zahariev and M. S. Gordon, *Journal of Physical Chemistry A*, **2011**, 115, 9801–9809.

41. J. Schirmer, *Phys Rev A (Coll Park)*, **1982**, 26, 2395.

42. A. B. Trofimov and J. Schirmer, *Journal of Physics B: Atomic, Molecular and Optical Physics*, **1995**, 28, 2299.

43. M. Falkowska, D. T. Bowron, H. G. Manyar, C. Hardacre and T. G. A. Youngs, *ChemPhysChem*, **2016**, 17, 2043–2055.

44. C. Di Mino, A. J. Clancy, A. Sella, C. A. Howard, T. F. Headen, A. G. Seel and N. T. Skipper, *J Phys Chem B*, **2023**, 127, 1357–1366.

45. P. K. Zarzycki, M. B. Zarzycka, M. M. Ślączka and V. L. Clifton, *Anal Bioanal Chem*, **2010**, 397, 905–908.

46. T. Yanai, D. P. Tew and N. C. Handy, *Chem Phys Lett*, **2004**, 393, 51–57.

47. D. Rappoport and F. Furche, *Journal of Chemical Physics*, **2010**, 133, 134105.

48. F. Weigend and R. Ahlrichs, *Physical Chemistry Chemical Physics*, **2005**, 7, 3297–3305.

49. M. J. Frisch, G. W. Trucks, H. B. Schlegel, G. E. Scuseria, M. A. Robb, J. R. Cheeseman, G. Scalmani, V. Barone, G. A. Petersson, H. Nakatsuji, X. Li, M. Caricato, A. Marenich, J. Bloino, B. G. Janesko, R. Gomperts, B. Mennucci, H. P. Hratchian, J. V. Ortiz, A. F. Izmaylov, J. L. Sonnenberg, D. Williams-Young, F. Ding, F. Lipparini, F. Egidi, J. Goings, B. Peng, A. Petrone, T. Henderson, D. Ranasinghe, V. G. Zakrzewski, J. Gao, N. Rega, G. Zheng, W. Liang, M. Hada, M. Ehara, K. Toyota, R. Fukuda, J. Hasegawa, M. Ishida, T. Nakajima, Y. Honda, O. Kitao, H. Nakai, T. Vreven, K. Throssell, J. A. Montgomery Jr., J. E. Peralta, F. Ogliaro, M. Bearpark, J. J. Heyd, E. Brothers, K. N. Kudin, V. N. Staroverov, T. Keith, R. Kobayashi, J. Normand, K. Raghavachari, A. Rendell, J. C. Burant, S. S. Iyengar, J. Tomasi, M. Cossi, J. M. Millam, M. Klene, C. Adamo, R. Cammi, J. W. Ochterski, R. L. Martin, K. Morokuma, O. Farkas, J. B. Foresman and D. J. Fox, **2013**.

50. V. Barone and M. Cossi, *Journal of Physical Chemistry A*, **1998**, 102, 1995–2001.

51. M. Cossi, N. Rega, G. Scalmani and V. Barone, *J Comput Chem*, **2003**, 24, 669–681.

52. S. G. Balasubramani, G. P. Chen, S. Coriani, M. Diedenhofen, M. S. Frank, Y. J. Franzke, F. Furche, R. Grotjahn, M. E. Harding, C. Hättig, A. Hellweg, B. Helmich-Paris, C. Holzer, U. Huniar, M. Kaupp, A. Marefat Khah, S. Karbalaei Khani, T. Müller, F. Mack, B. D. Nguyen, S. M. Parker, E. Perlt, D. Rappoport, K. Reiter, S. Roy, M. Rückert, G. Schmitz, M. Sierka, E. Tapavicza, D. P. Tew, C. Van Wüllen, V. K. Voora, F. Weigend, A. Wodyński and J. M. Yu, *J Chem Phys*, **2020**, 152, 184107.

53. Y. J. Franzke, C. Holzer, J. H. Andersen, T. Begušić, F. Bruder, S. Coriani, F. Della Sala, E. Fabiano, D. A. Fedotov, S. Fürst, S. Gillhuber, R. Grotjahn, M. Kaupp, M. Kehry, M. Krstić, F. Mack, S. Majumdar, B. D. Nguyen, S. M. Parker, F. Pauly, A. Pausch, E. Perlt, G. S. Phun, A. Rajabi, D. Rappoport, B. Samal, T. Schrader, M. Sharma, E. Tapavicza, R. S. Treß, V. Voora, A. Wodyński, J. M. Yu, B. Zerulla, F. Furche, C. Hättig, M. Sierka, D. P. Tew and F. Weigend, *J Chem Theory Comput*, **2023**, 19, 6859–6890.

54. A. Klamt and G. Schüürmann, *Journal of the Chemical Society, Perkin Transactions 2*, **1993**, 799–805.

55. B. Lunkenheimer and A. Köhn, *J Chem Theory Comput*, **2013**, 9, 977–994.

56. A. Dreuw and M. Wormit, *Wiley Interdiscip Rev Comput Mol Sci*, **2015**, 5, 82–95.

57. G. Braun, I. Borges, A. J. A. Aquino, H. Lischka, F. Plasser, S. A. Do Monte, E. Ventura, S. Mukherjee and M. Barbatti, *Journal of Chemical Physics*, **2022**, 157, 154305.

58. T. M. Cardozo, A. J. A. Aquino, M. Barbatti, I. Borges and H. Lischka, *Journal of Physical Chemistry A*, **2015**, 119, 1787–1795.

59. I. Borges, A. J. A. Aquino, M. Barbatti and H. Lischka, *Int J Quantum Chem*, **2009**, 109, 2348–2355.

60. I. Borges, A. J. A. Aquino, A. Köhn, R. Nieman, W. L. Hase, L. X. Chen and H. Lischka, *J Am Chem Soc*, **2013**, 135, 18252–18255.

61. I. Borges, E. Uhl, L. Modesto-Costa, A. J. A. Aquino and H. Lischka, *Journal of Physical Chemistry C*, **2016**, 120, 21818–21826.

62. S. A. Mewes, F. Plasser, A. Krylov and A. Dreuw, *J Chem Theory Comput*, **2018**, 14, 710–725.

63. T. M. Cardozo, A. P. Galliez, I. Borges, F. Plasser, A. J. A. Aquino, M. Barbatti and H. Lischka, *Physical Chemistry Chemical Physics*, **2019**, 21, 13916–13924.

64. D. De Castro Araujo Valente, I. Borges and T. M. Cardozo, *Physical Chemistry Chemical Physics*, **2021**, 23, 26561–26574.

65. R. S. Mattos, I. Burghardt, A. J. A. Aquino, T. M. Cardozo and H. Lischka, *J Am Chem Soc*, **2022**, 144, 23492–23504.

66. L. Modesto-Costa, E. Uhl and I. Borges, *J Comput Chem*, **2015**, 36, 2260–2269.

67. M. V. Bohnwagner, I. Burghard and A. Dreuw, *Journal of Physical Chemistry A*, **2016**, 120, 14–27.

68. L. Modesto-Costa and I. Borges, *Spectrochim Acta A Mol Biomol Spectrosc*, **2018**, 201, 73–81.

69. R. L. Martin, *J Chem Phys*, **2003**, 118, 4775–4777.

70. F. Plasser, *Journal of Chemical Physics*, **2020**, 152.

71. F. Plasser, **2016**.

72. S. A. Bäppler, F. Plasser, M. Wormit and A. Dreuw, *Phys Rev A*, **2014**, 90, 052521.

73. F. Plasser and H. Lischka, *J Chem Theory Comput*, **2012**, 8, 2777–2789.

74. K. N. Trueblood, E. Goldish, J. Donohue and IUCr, *Acta Crystallogr*, **1961**, 14, 1009–1017.

75. M. Colapietro, A. Domenicano, C. Marciante and G. Portalone, *Zeitschrift fur Naturforschung - Section B Journal of Chemical Sciences*, **1982**, 37, 1309–1311.

76. Nieger. M. and CCDC, **2008**.

77. S. Narra, S. W. Chang, H. A. Witek and S. Shigeto, *Chemistry – A European Journal*, **2012**, 18, 2543–2550.

78. S. A. Kovalenko, R. Schanz, V. M. Farztdinov, H. Hennig and N. P. Ernsting, *Chem Phys Lett*, **2000**, 323, 312–322.

79. K. Mohanalingam and H. o. Hamaguchi, *Chem Lett*, **2004**, 157–158.

80. C. L. Thomsen, J. Thøgersen and S. R. Keiding, *Journal of Physical Chemistry A*, **1998**, 102, 1062–1067.

81. B. J. C. Cabral, R. Rivelino, K. Coutinho and S. Canuto, *Journal of Physical Chemistry B*, **2015**, 119, 8397–8405.

82. M. Máximo-Canadas and I. Borges, *Zenodo*, **2023**. DOI: 10.5281/zenodo.10524944